Journal of Fluids and Structures (2002) **16**(3), 417–433
doi:10.1006/jfls.2000.0428, available online at http://www.idealibrary.com on IDEAL®

SELF-INDUCED SLOSHING CAUSED BY AN UPWARD ROUND JET IMPINGING ON THE FREE SURFACE

H. MADARAME, K. OKAMOTO AND M. IIDA†

Nuclear Engineering Research Laboratory, University of Tokyo, Tokai-mura, Naka-gun Ibaraki 319-1188, Japan

(Received 28 August 2000, and in final form 12 June 2001)

Self-induced sloshing was found to occur in a cylindrical tank when an upward round jet on the tank axis created a surface swell at the impingement point. The conditions under which the sloshing occurred were investigated experimentally, together with the sloshing modes and frequencies. The sloshing was found to appear when the inlet velocity exceeded a certain value, which depends on the inlet-surface distance. The mode always had one diametrical node, and a lower mode appeared at increased inlet-surface distance and velocity. A feedback model was proposed in order to explain the energy supply mechanism to the sloshing, which was composed of a jet deflection process caused by a lateral pressure gradient and a pressure imbalance generation process caused by jet movement. The lateral pressure gradient deflects the jet, resulting in the displacement of the surface impingement point. When the jet moves, transformation of the jet-induced swell does not follow the movement immediately, generating an imbalance of pressure. The imbalance caused by the motion of the swell is considered to supply energy to the sloshing. The calculated jet deflection caused by the lateral pressure gradient was found to agree with the experimental findings. The measured lateral pressure gradient was calculated as the sum of the lateral pressures caused by the sloshing motion and by the jet impingement point movement. The calculated oscillating region in the water-depth jet-velocity map was found to agree fairly well with the experimental findings, which suggests the validity of the model.

1. INTRODUCTION

THE AUTHORS HAVE CONDUCTED a number of studies on self-induced free surface oscillations caused by circulating flow in rectangular and cylindrical tanks (Okamoto & Madarame 1998). A self-induced sloshing was observed in a cylindrical tank having a submerged round jet on the tank axis impinging on the free surface (Madarame *et al.* 1995). When an upward plane jet in a rectangular tank impinged on the free surface, two types of oscillation appeared: "self-induced sloshing" (Fukaya *et al.* 1996) and "jet-flutter" (Madarame & Iida 1998). The frequency of the former was indicative of sloshing, whereas that of the latter was indicative of water oscillation in a U-tube of the same depth. Sloshing was induced in the cylindrical tank by the jet, the frequency of which was not a U-tube water oscillation. However, the similarity of the frequency governing mechanism does not necessarily imply similarity with respect to energy supply mechanism. The self-induced sloshing in the rectangular tank appeared in narrow belt-shaped regions, whereas the jet-flutter appeared over a wide region of the water-depth jet-velocity map. This is due to the different energy supply mechanisms of the oscillations. A surface swell was found to play an important role

†Iida Tekko Inc.

0889–9746/02/030417 + 17 $35.00/0

in the latter case, whereas no swell formed clearly in the former case. Unlike the self-induced sloshing in the rectangular tank, the self-induced sloshing in the cylindrical tank appeared over a wide region of the water-depth jet-velocity map. A surface swell was formed by the jet impingement in the cylindrical tank.

In the present study, the characteristics of the sloshing in a cylindrical tank are examined in detail. The feedback model developed to explain the energy supply mechanism to jet-flutter (Madarame & Iida 1998) is then applied to the cylindrical tank. Through comparison of the analytical and experimental results, the energy supply mechanism to sloshing in the cylindrical tank is discussed.

A small upward round jet impinging on the free surface has been reported to oscillate under certain conditions (Houard *et al.* 1998). Although the geometrical arrangement of the experimental apparatus used by Houard is similar to that used in the present experiment, the mechanism of the oscillation is completely different. The small jet oscillation is no longer observed for jet diameters larger than 2·5 mm, nor is it observed at depths greater than 3 cm. The self-induced sloshing in the cylindrical tank is induced by a jet of 25 or 50 mm diameter. The capillary force plays an important role in the small jet oscillation, whereas no meaningful effect of the surface tension is observed in self-induced sloshing.

2. EXPERIMENT

2.1. Experimental Apparatus

Schematic and cross-sectional views of the cylindrical tank are shown in Figure 1. The cylindrical tank consisted of two coaxial cylinders, both of which were of 5 mm thick transparent acrylic resin. The outer cylinder (inner diameter of 800 mm) was set on the base plate, the bottom plate of the tank. Water depth in the tank was controlled by the height of the outer cylinder in the range from 100 to 500 mm. In the present paper, the outer cylinder height was used as the water depth, because the water depth was only a few millimetres larger than the outer cylinder height, except in thick-inlet-pipe and high-velocity cases. The difference was only 1 or 2 cm even in the exceptional cases and thus can be neglected when considering the measurement interval of 500 mm. The inner cylinder was inserted into the outer cylinder from above. The distance from the tank bottom to the lower edge of the inner cylinder was maintained at 50 mm in order to form an underflow gate between them. The purpose of the inner cylinder was to insulate the inside water surface from the influence of outflow over the outer cylinder. The jet inlet pipe of 25 or 50 mm inner diameter and 500 mm length was set at the centre of the tank bottom, which could extend into the tank to a height of up to 350 mm.

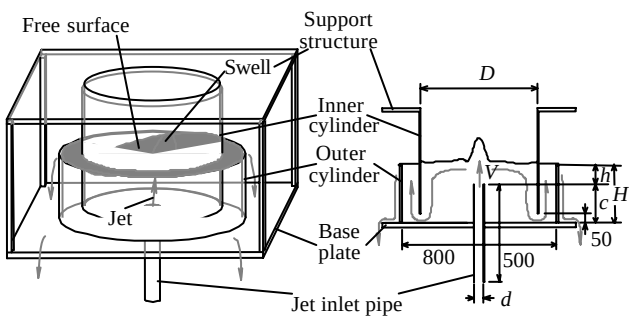

Figure 1. Test tank; dimensions in mm.

TABLE 1
Experimental parameters
Range of variable parameters H, h: 50–400 m/s; u_0: 0–4·1 m/s

	Diameter of inner cylinder (mm)	Diameter of jet inlet pipe (mm)	Fixed parameter (mm)	Variable parameters
A	$D = 600$	$d = 25$	$H = 400$	h, u_0
B	600	25	$c = 0$	H, u_0
C	300	25	$H = 400$	h, u_0
D	600	50	$H = 400$	h, u_0

Water entered the tank as a submerged round jet. The jet impinged on the free surface, where a swell was formed, and then spread outwards. Water flowed down along the inner cylinder wall, passed through the underflow gate to the annulus between the cylinders, and overflowed from the tank. Since water was supplied from a head tank having a constant water level, no pump pulsation influenced the jet. The inlet velocity of the jet was calculated based on the flow rate as measured by a rotameter. The water level fluctuation in the tank was measured by a condenser-type level meter installed at a location 50 mm inside the inner cylinder wall. Frequencies of the oscillation were obtained by fast Fourier transfer analysis of the water level fluctuation.

The inner diameter of the inner cylinder, D, the inner diameter of the inlet pipe, d, the water depth, H, the protruded length of inlet into the tank, c, and the inlet velocity, u_0, were varied as shown in Table 1 in order to clarify their effects on the oscillation. The sloshing was induced when the Reynolds number at the jet inlet pipe was greater than approximately 8000, i.e., a turbulent jet. The difference between H and c gave the distance from the inlet to the free surface, h. In obtaining accurately the occurrence map of oscillation, the inlet velocity was maintained at zero until the surface fluctuation was completely suppressed before adjusting to the designated value. The judgement of the oscillation growth and the mode was performed several minutes after the adjustment so as to exclude transient phenomena. When the sloshing amplitude near the wall was larger than 10 mm, the system was considered to be in oscillation.

2.2. SURFACE BEHAVIOUR

Water injection into the tank formed a swell at the impingement point on the free surface. When the inlet velocity exceeded a certain value, the swell oscillated laterally in a diametral plane or rotated around the tank axis. The surrounding water sloshed synchronously with the swell.

Sketches of the oscillating water surface are shown in Figure 2. Figure 2(a) and 2(b) shows the oscillation in the direction perpendicular to a diametral plane, accompanied by sloshing of the surrounding water in the same direction. The sloshing mode was found to always have only one diametral node and at least one circular node at the inner cylinder wall. In the following, the mode having n circular nodes, including the inner cylinder wall, is called the nth mode, i.e., Figure 2(a) depicts the first mode and Figure 2(b) the second mode. The oscillation occasionally changed direction, either steadily or randomly, forming a spiral or more complex waves on the surrounding surface, as illustrated in Figure 2(c). A swell approximately 500 mm in height, as shown in Figure 2(d), was observed at the maximum flow rate. The appearance of this swell was similar to what may be observed in a fountain in a park.

The swell and the surrounding water surface rotated around the tank axis in some cases. This rotation was caused by an oscillation in a plane superimposed on another oscillation of

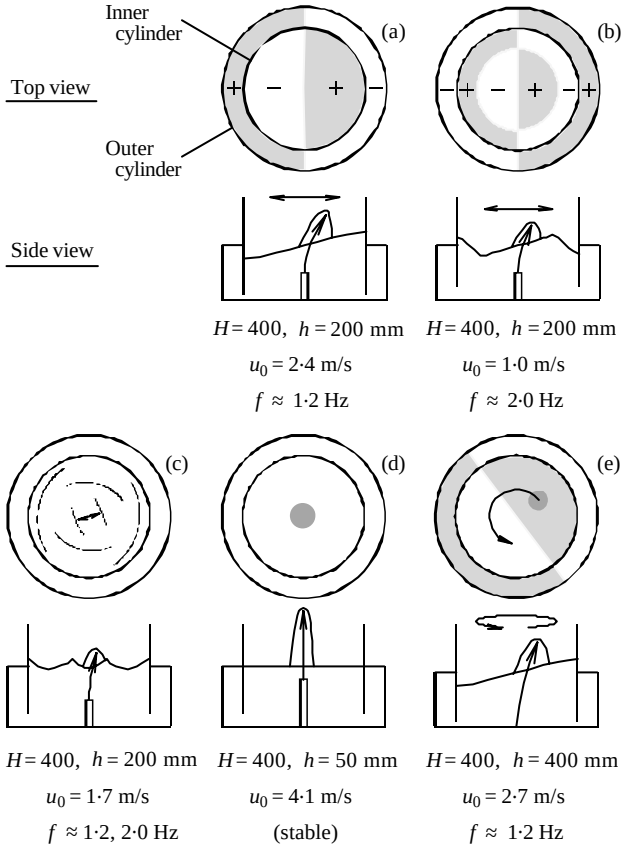

Figure 2. Sketches of oscillating water surface.

the same mode in the perpendicular direction, which was not accompanied by a substantial circulating flow in the tank. Only the first mode was observed clearly to cause the rotation, as shown in Figure 2(e). The rotation was not induced accidentally by an uncontrollable initial condition, but rather was always induced under the appropriate conditions. Without exception, the swell leaned towards the rising gradient of the sloshing surface during the rotation as well as during the one-directional oscillation.

2.3. Measured Frequency

The frequency spectrum had one or two dominant peaks, as shown in Figure 3. The peaks were determined by the inner cylinder diameter (1·2, 2·0 and 2·5 Hz when $D = 600$ mm, and 1·8 and 3·0 Hz when $D = 300$ mm), which agreed well with natural frequencies of sloshing in the tank. These frequencies were close to the values calculated by the following equation, except for shallow-water cases:

$$f = \frac{1}{2\pi}\sqrt{\frac{k_n g}{R}\tanh\left(\frac{k_n H}{R}\right)} \quad (n = 1, 2, \ldots) \tag{1}$$

where R ($=D/2$) is the radius of the inner cylinder, g is the gravitational acceleration and k_n is the nth root of the derivative of the first-order Bessel function, $J_1'(k_n) = 0$. A coupling

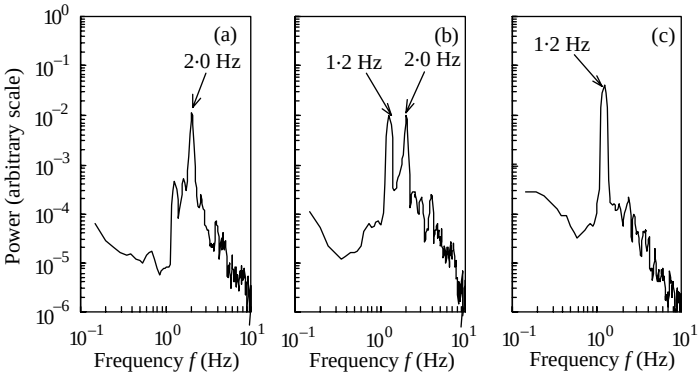

Figure 3. Examples of frequency spectrum (Case D, $h = 200$ mm); (a) $u_0 = 1{\cdot}0$ m/s; (b) $u_0 = 1{\cdot}7$ m/s; (c) $u_0 = 2{\cdot}4$ m/s.

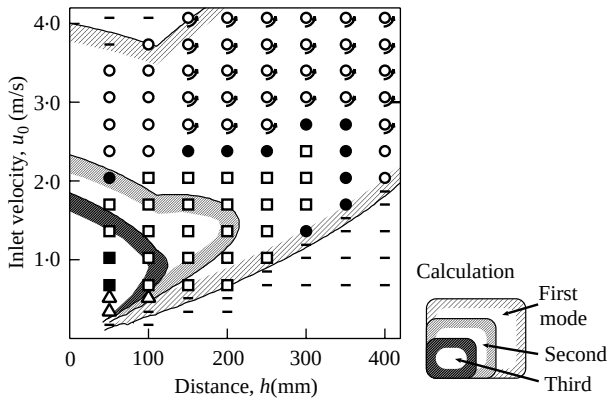

Figure 4. Osillating condition, case A; Experiment: ○, 1·2 Hz (first mode); ●, 1·2, 2·0 Hz; □, 2·0 Hz (second mode); ■, 2·0, 2·5 Hz; △, 2·5 Hz (third mode); —, stable; ↻, rotation.

effect with water motion in the annulus region between the cylinders could not be ignored in shallow-water cases.

When the single peak of 2·0 Hz in Figure 3(a) appeared, the second mode in Figure 2(b) was observed. The single peak of 1·2 Hz in Figure 3(c) corresponds to the first mode in Figure 2(a). Under the condition in which two peaks coexist, as shown in Figure 3(b), complex waves, illustrated in Figure 2(c), were formed on the surface due to interference of two different modes.

2.4. Measured Oscillating Region

The oscillating regions in all cases are shown in Figures 4–7. The dominant frequencies are also indicated using different symbols. The self-induced oscillation appeared when the inlet velocity exceeded a certain limit, which increased with increasing distance from the inlet to the free surface. Oscillation including rotation was induced even at the maximum flow rate, which was limited by the capacity of the apparatus, except in the case for which the distance was so short that the stable fountain shown in Figure 2(d) appeared.

The dominant frequency shifted lower in discrete steps (e.g., from 2·5 through 2·0 to 1·2 Hz) with increasing distance and velocity. Between two regions having different single

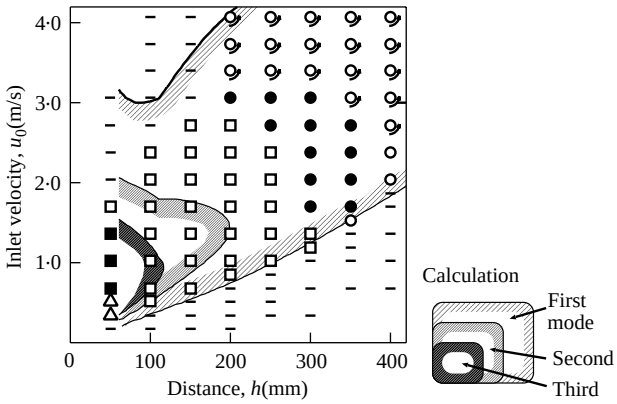

Figure 5. Oscillating condition, case B; $H = h$. Experiment: ○, 1·2 Hz (first mode); ●, 1·2, 2·0 Hz; □, 2·0 Hz (second mode); ■, 2·0, 2·5 Hz; △, 2·5 Hz (third mode); —, stable; ↗, rotation.

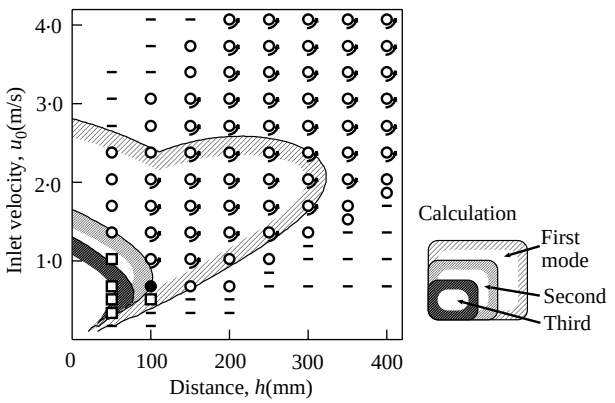

Figure 6. Oscillating condition, case C; $D = 300$ mm. Experiment: ○, 1·8 Hz (first mode); ●, 1·8, 3·0 Hz; □, 3·0 Hz (second mode); —, stable; ↗, rotation.

dominant frequencies, the two frequencies coexisted. The rotation was more stable than the one-directional oscillation in the marked region shown in Figures 4–7, i.e., the rotation appeared eventually, regardless of initial conditions. The rotation required a greater distance and velocity than the one-directional oscillation, and appeared in a wider region in the small inner cylinder case (Case C). One-directional excitation is known to cause rotary sloshing under certain conditions by a nonlinear effect (Abramson *et al.* 1966). The nonlinear effect is considered to cause the rotation in the self-induced sloshing; however, further discussion is beyond the scope of the present study.

The distance from the inlet to the free surface, h, was used to draw the oscillating region maps in Figures 4–7. The use of h gave a similar velocity limit of oscillating region and shift of dominant frequency for Case A and Case B, which suggests that the oscillating region and the mode are governed not by H, but rather by h. However, the oscillation of 1·2 Hz was induced at a distance of approximately 100 mm and a velocity of approximately 3·0 m/s in Case A, whereas no oscillation appeared under the same conditions in Case B. The reason for this difference was explained by the result of a forced oscillation experiment that was performed without the jet, which revealed that the first mode was damped down quickly when the water depth, H, was small. When H was small, the water level in the annulus

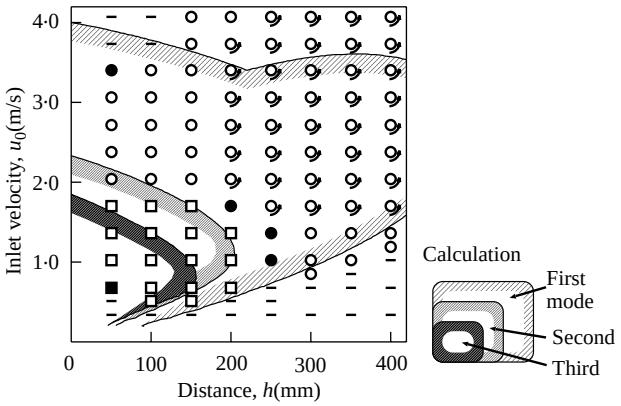

Figure 7. Oscillating condition, case D; $d = 50$ mm. Experiment: ○, 1·2 Hz (first mode); ●, 1·2, 2·0 Hz; □, 2·0 Hz (second mode); ■, 2·0, —, stable; ↻, rotation.

oscillated considerably coupled with the sloshing inside the inner cylinder, as mentioned previously. The intermittent outflow over the outer cylinder was considered to damp down the sloshing in this region.

Figure 6 shows the result of Case C, in which the inner cylinder diameter was reduced to 300 mm. The lower velocity limit for oscillation growth was approximately the same as that in Case A. Although the frequency in Case C was different from that in Case A, a similar tendency to shift down in discrete steps with increasing distance and velocity was observed. Over the greater part of the oscillating region, the first mode having a single frequency of 1·8 Hz appeared, which in most cases rotated in the tank.

The effect of jet diameter was examined in Case D by doubling the inlet pipe diameter, as shown in Figure 7. The lower velocity limit in this case decreased, compared with Case A. The region of 1·2 Hz, as well as that of rotation, extended to lower velocities.

2.5. Surface Motion, Pressure Change and Jet Behaviour

In order to determine the causal sequence of fluctuating quantities in the phenomenon, the relationship among the surface motion, the lateral pressure gradient across jet and the displacement of jet was examined. The measurement was performed for Case A′, as shown in Figure 8, in which the water depth, H, was changed to 500 mm from 400 mm. The protruded length of the inlet into the tank, c, was 100 mm, and the inlet velocity, u_0, was 2·38 m/s. Under this condition, the first mode of sloshing without rotation appeared. The outer cylinder was replaced by a square tank having sides of 800 mm length so as to make visualization of the jet possible. The diametral plane of oscillation was fixed parallel to the square tank wall by dipping a 5 mm thick plate into the water at a distance of approximately 100 mm from the surface. The pressure difference across the jet was measured using pressure taps installed 20 mm above the jet inlet. The distance between the taps was 125 mm.

The surface motion and the pressure difference across the jet are shown in Figure 9. The surface level was measured not on the cylinder wall, but rather 50 mm inside the wall. These surface-level measurements were found to be approximately equal. The amplitude was approximately 20 mm, which was calculated to cause a 15 Pa pressure difference between the measurement points changing in phase. The amplitude of the measured pressure difference was found to be as large as 60 Pa, and the phase was found to be 52° behind the

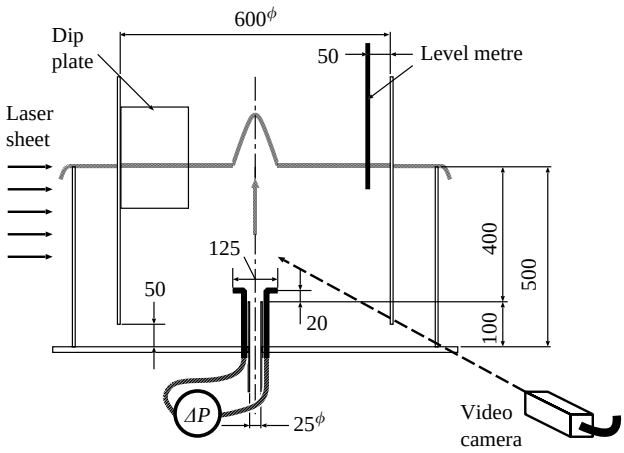

Figure 8. Measuring system; dimensions in mm.

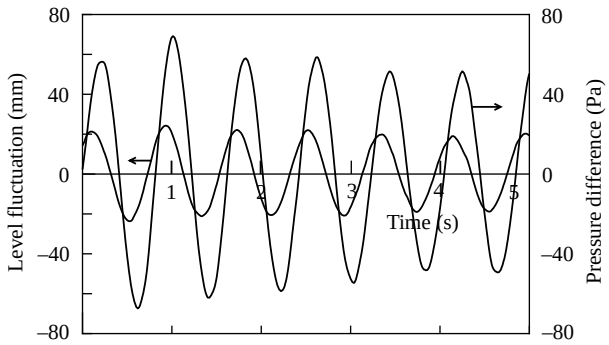

Figure 9. Level fluctuation and pressure difference.

surface motion. These results indicate that the lateral pressure gradient acting on the jet was not only governed by the sloshing motion, but was also affected by other mechanisms.

The displacement of jet was visualized using a fluorescent dye and a laser sheet. The jet without the dye did not fluoresce on laser exposure, and so was distinguishable from the fluorescent surrounding water. Approximating the horizontal brightness variation by the Gaussian distribution and taking the maximum point, the displacement of the jet centre was obtained. In order to eliminate noise, the displacement was measured during several periods and the variation of the position was approximated by a sinusoidal curve. The amplitude and phase of the displacement at each elevation are shown in Figure 10, where the phase was determined on the basis of pressure change. An immediate response of the jet to the pressure change is expressed by a phase lag of -180°, because the jet is pushed to the opposite direction of the pressure gradient. Therefore, the phase lag increased from -180° toward 0°.

The surface contour on the diametral plane of oscillation is shown in Figure 11. The swell position is marked by a broad arrow. The phase of the swell position was 4° behind the level metre signal, and 48° ahead of the pressure difference. The phase of the swell position is almost on the extension of the jet displacement phase-location line, as shown in Figure 10.

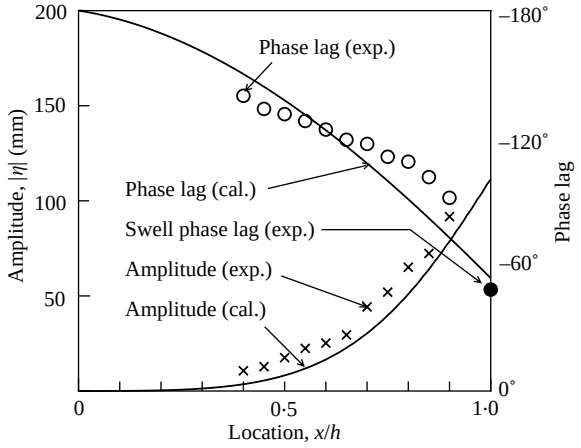

Figure 10. Jet displacement.

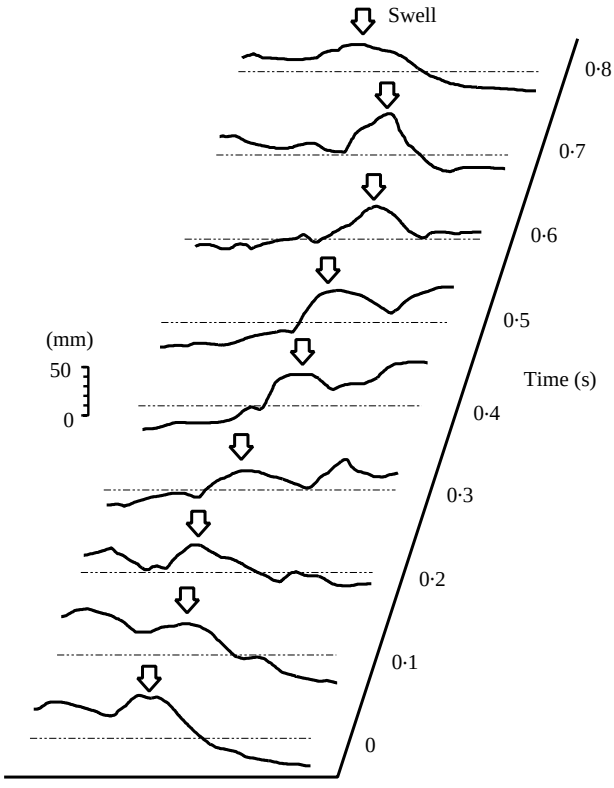

Figure 11. Surface contour.

3. ANALYSIS

3.1. Energy Supply Mechanism for Sloshing

In a sloshing system, surface deformation causes unbalanced pressure distribution in the water. The pressure moves the water, which causes the surface deformation. Thus, a

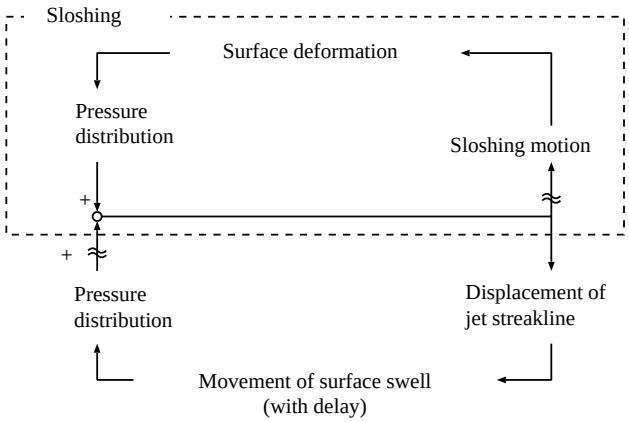

Figure 12. Feedback model.

feedback loop is constituted in an ordinary sloshing, as illustrated in the dotted box of Figure 12. In self-induced sloshing, there exists another feedback mechanism, which is illustrated outside the dotted box. The lateral pressure gradient not only causes the sloshing motion, but also deflects the jet, which results in the displacement of the surface impingement point. The jet possessing upward momentum at the surface forms a swell at the impingement point, and loses the momentum in the swell, receiving the gravitational acceleration. Since the gravity is not balanced by the pressure gradient, but rather by the deceleration of the water in the swell, the pressure beneath the swell is not necessarily higher than that of the surroundings. When the jet forming the swell moves laterally, transformation of the swell cannot follow the movement instantaneously. A pressure imbalance occurs, low pressure at the front and high pressure at the rear. The sloshing grows for the case in which the pressure imbalance operates to promote the sloshing motion by a positive feedback effect.

In the actual case, the jet streak-line is affected not only by the pressure imbalance, but also by the pressure gradient caused by the sloshing motion. Calculating the streak-line is not easy, considering the feedback effect. In the following, we break the loop at the wavy line positions in the figure and examine the open-loop transfer function rather than that of the closed loop.

3.2. Numerical Simulation of Jet behaviour

The velocity potential of the sloshing can be expressed as the following equation, taking the origin as the jet inlet, the x-axis in the upward direction and the r-axis in the radial direction, as shown in Figure 13 (Lamb 1932):

$$\Phi = \frac{Ag}{\omega} \frac{\mathrm{J}_1(k_n r/R)}{|\mathrm{J}_1(k_n)|} \frac{\cosh(k_n(x + H - h)/R)}{\cosh(k_n H/R)} \cos\theta \sin\omega t, \quad n = 1, 2, \ldots \tag{2}$$

where A is the amplitude of surface motion at $r = R$. The angular frequency, $\omega = 2\pi f$, is given by equation (1). Although two or more modes of sloshing were occasionally found to coexist during the experiment, only a single mode of sloshing is treated here. Substituting equation (2) into Bernoulli's equation, the r-directional pressure gradient at $\theta = 0$, i.e., the

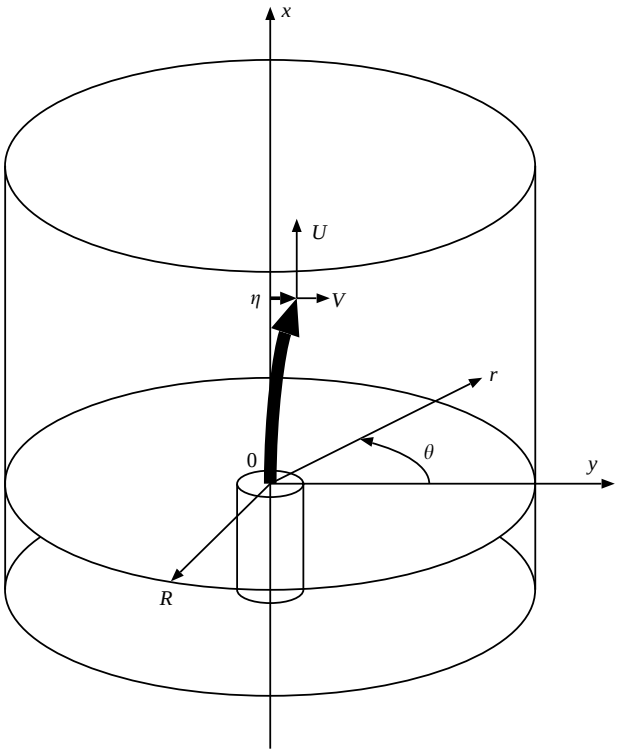

Figure 13. Coordinate system.

y-directional gradient at $y = 0$, is obtained as follows:

$$\left.\frac{\partial p}{\partial y}\right|_{y=0} = -\frac{A\rho g}{2R}\frac{k}{|\mathrm{J}_1(k)|}\frac{\cosh(k(x+H-h)/R)}{\cosh(kH/R)}\cos\omega t, \tag{3}$$

where ρ is the water density. The dynamic pressure, which is low compared to the static pressure, is neglected.

The lateral displacement of the jet, η, can be calculated by the following equations (Nyborg 1954):

$$\eta(x,t) = \int_{t-\tau}^{t} (t-t')\frac{\mathrm{d}V}{\mathrm{d}t'}\,\mathrm{d}t', \qquad \tau(x) = \int_0^x \frac{\mathrm{d}x'}{U(x')}, \tag{4, 5}$$

where U and V are representative x- and y-direction velocity components of the jet, respectively. Assuming small amplitude, the y-direction acceleration acting on the jet is described by the following equation:

$$\frac{\mathrm{d}V}{\mathrm{d}t} = -\frac{1}{\rho}\left.\frac{\partial p}{\partial y}\right|_{y=0}. \tag{6}$$

The velocity at the jet axis, u_m, can be approximated as follows (Abramovich 1963):

$$u_m(x) = -\frac{0{\cdot}96u_0}{2a(x-x_p)/d}, \tag{7}$$

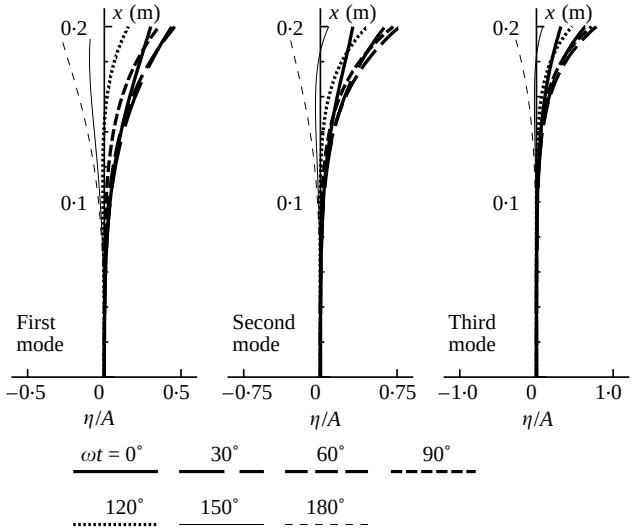

Figure 14. Calculated streak-lines for $u_0 = 2{\cdot}0$ m/s and $h = 0{\cdot}2$ m.

where $a = 0{\cdot}076$ is an experimental constant and $x_p = -0{\cdot}29d/2a$ is the pole position. When a jet receives a transverse force, particles at different distances from the jet centre have different path-lines that intersect each other. The mixing motion intensifies the turbulence, and a disturbance having a certain wave speed propagating in the axial direction grows there. The wave speed is roughly the same as the velocity at the point at which the velocity gradient is steepest. Thus, we assume the following (Blake 1986):

$$U(x) = 0{\cdot}5u_m(x). \tag{8}$$

Using equations (1)–(8), we can obtain the movement of jet by the Runge–Kutta method. The calculated result in Case A is shown in Figure 14.

The acceleration $\mathrm{d}V/\mathrm{d}t$ is maximum at $\omega t = 0$. If the jet displacement responds to the periodic acceleration instantaneously, the jet moves to the right, the positive direction of y, at $\omega t = 0$. However, the jet displacement is affected by the previous acceleration profile on the upstream path, which causes a phase lag. The displacement of the surface impingement point is maximum near $\omega t = 60^\circ$ in Figure 14. The phase lag increases with increasing time required for the jet to travel from the inlet to the surface due to the substantial effect of previous acceleration. This does not necessarily mean that the phase lag is large in a higher mode having a short period. In higher modes, the acceleration caused by the sloshing is very small near the bottom. The displacement is large only in the vicinity of the surface. The memory effect is small, sometimes resulting in the phase lag of the third mode being smaller than that of the second mode. The jet displacement at the surface position, $x = h$, can be expressed by the following equation:

$$\eta_h = \varepsilon A \cos(\omega t - \varphi_1), \tag{9}$$

where εA denotes the amplitude and φ_1 denotes the phase lag behind the acceleration oscillation.

3.3. Pressure Gradient Caused by Movement of Impinging Point

Although the jet velocity is distributed in the lateral direction, we assume that a jet having a uniform velocity u_m and a radius of σ reaches the surface position, $x = h$. The imbalance

between the swell shape and the momentum supply by the jet is generated only at the jet periphery, $r = \sigma$, when we assume infinitesimal amplitude. The amount of generated imbalance is as follows:

$$q(t, \theta) = -\frac{\rho u_h^2}{2} \frac{\partial}{\partial t} \eta_h\left(t - \frac{u_h}{g}\right) \cos\theta = \varepsilon\omega A \frac{\rho u_h^2}{2} \sin(\omega t - \varphi_1 - \varphi_2)\cos\theta, \tag{10}$$

where $\varphi_2 = \omega u_h/g$ is the phase lag due to the time required for the jet to lose upward momentum in the swell. The mass of the jet begins to contribute to the hydraulic head in the position after losing the upward momentum. The pressure imbalance is attenuated after a certain time, generating local motion of water. The motion propagates outward as a wave. The localized imbalance raises a wave of a short wavelength; thus, the propagation speed of the wave is low. The speed of the wave attenuating the imbalance is sufficiently low compared to the sloshing wavelength divided by the sloshing period. Therefore, neglecting the attenuating wave does not produce a serious error when we estimate the effect of the imbalance on the sloshing growth. The force acting on the sloshing motion at each moment is the time integral of equation (10):

$$F(t, \theta) = \varepsilon A \frac{\rho u_h^2}{2} \cos(\omega t - \varphi_1 - \varphi_2)\cos\theta. \tag{11}$$

The force acts at $r = \sigma$ in the positive direction of x. The vertical motion of the sloshing surface at $r = \sigma$ is expressed as

$$\left.\frac{\mathrm{d}\zeta}{\mathrm{d}t}\right|_{r=\sigma} = \frac{\omega A\sigma}{2R} \frac{k}{|\mathrm{J}_1(k)|} \cos\theta \sin\omega t, \tag{12}$$

where we assume $\sigma \ll R$. The energy supplied to the sloshing in a period is calculated as follows:

$$\Delta E = \oint \int_0^{2\pi} \left.\frac{\mathrm{d}\zeta}{\mathrm{d}t}\right|_{r=\sigma} F\sigma \,\mathrm{d}\theta \,\mathrm{d}t = \frac{\pi^2 \varepsilon A^2 \rho u_h^2 \sigma^2}{4R} \frac{k}{|\mathrm{J}_1(k)|} \sin(\varphi_1 + \varphi_2). \tag{13}$$

Thus, the oscillation condition is given as follows:

$$\sin(\varphi_1 + \varphi_2) > 0. \tag{14}$$

3.4. Oscillating Region

Figure 15 shows the phase lag of the jet impingement point behind the periodic lateral acceleration, φ_1, and the lag caused by the required time for the jet to lose momentum, φ_2, in the first mode of Case A. The phase lag φ_1, illustrated by solid lines, is 0 at $h = 0$, and increases with increasing h/u. Theoretically, the phase lag increases indefinitely. The value up to 210° is shown in the figure. φ_2 illustrated by broken lines is 0 at $u_0 = 0$, and increases with increasing u_0. The value of $u_m(h)$ calculated by equation (7) exceeds u_0 when h is very small. Since values of u_h that are greater than u_0 are physically meaningless, the lower value between u_0 and $u_m(h)$ given by equation (7) is used for u_h to calculate φ_2. The bend in the broken lines at approximately $h = 110$ mm reflects the switch from u_0 to $u_m(h)$.

The calculated oscillating region, i.e., $0° < \varphi_1 + \varphi_2 < 180°$, is illustrated and compared to the experimental region in Figures 4–7. The $360° < \varphi_1 + \varphi_2 < 540°$ regions in the calculation appear when h is very small or when u_0 is very large, which also satisfies the condition of equation (14). These regions are not shown in the figures because no oscillation was observed there. When the water depth H is small in Case B (Figure 5), the sloshing

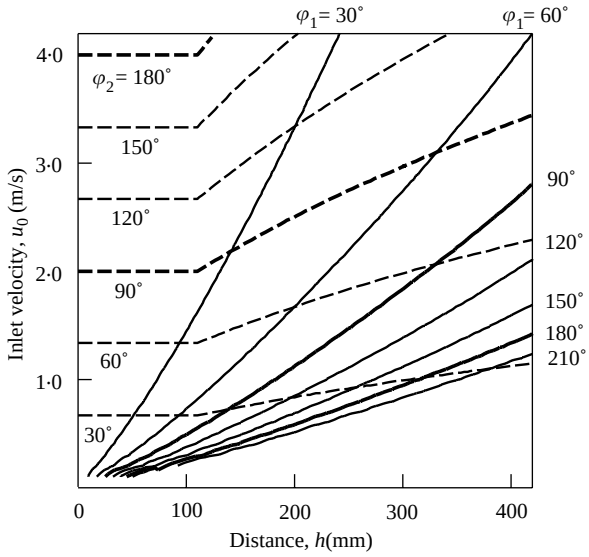

Figure 15. Phase lags.

frequency did not agree with the value calculated by equation (1) because of the coupled effect with water in the annulus region. Therefore, the frequency in Case B was obtained not by equation (1), but rather by numerical calculation.

In every case, the supplied energy is positive when the distance from the inlet to the surface, h, is not very large. For the inlet velocity, u_0, lower and upper limits of the oscillation region exist. The lower limit corresponds approximately to $\varphi_1 = 180°$. In other words, the phase lag of swell motion behind the periodical acceleration of less than 180° is a necessary condition of oscillation. In the large-inlet-pipe-diameter case (Case D), the jet velocity u_m does not decelerate quickly. The same inlet velocity gives a higher u_m than in Case A; therefore, the lower limit of the inlet velocity decreases in Case D. The upper limit is determined primarily by the condition of $\varphi_2 < 180°$. The time required for the jet to lose momentum in the swell increases with increasing swell height, $u_h^2/2g$. If this time is too long, energy is not supplied to the oscillation. A higher mode has a larger φ_2 for the same values of h and u_0, which is the reason why the higher modes have narrower regions. The low upper u_0 limit in Case C and in the first mode of Case B are also explained by this phenomenon.

4. DISCUSSION

4.1. Jet Behaviour

Equations (4)–(8) should hold for the measured value of the lateral pressure gradient, $\partial p/\partial y|_{y=0}$. The calculated displacement of jet is compared to the experimental value in Figure 10. For comparison, we assumed in the calculation the lateral pressure gradient 20 mm above the inlet to be 60 Pa/125 mm = 480 Pa/m. For the vertical distribution of the pressure, equation (3) was assumed. The calculated results agree with the experimental results; thus, we conclude that the jet displacement is calculated accurately by equations (4)–(8).

4.2. Phase Relations

The open-loop transfer function was examined analytically by breaking the feedback loop at the wavy line positions in Figure 12 in order to obtain the oscillating region. In the actual

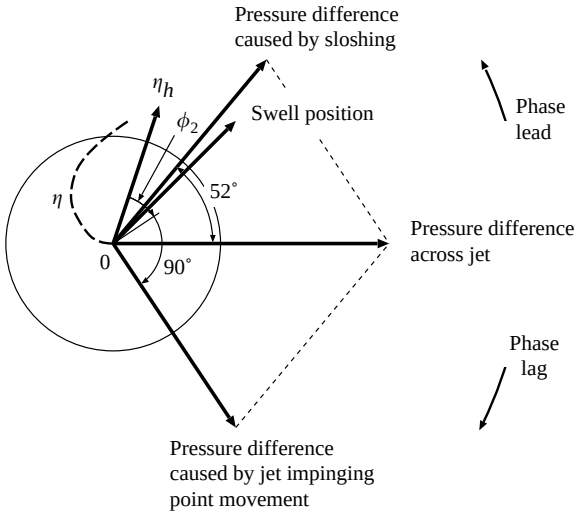

Figure 16. Phase relations.

case, the lateral pressure gradient, $\partial p/\partial y|_{y=0}$, is the sum of the lateral pressure gradient caused by the sloshing motion expressed by equation (3) and that caused by the jet impingement point movement. The summation should be performed considering the phase relation. Figure 16 illustrates the phase relations among the pressure differences, the jet displacement and the swell position. The pressure difference across the jet is the vector sum of those caused by the sloshing motion and by the jet impingement point movement. Thus, we can conclude that the feedback model in Figure 12 is valid.

4.3. Oscillating Region

The analytical result clarifies why the higher modes grow only in the low-u_0 low-h regions. According to the analysis, the first mode sloshing can grow even in the region in which higher modes grow. In the experiment, the first mode was suppressed when higher modes grew. The oscillation modes coexist because they are orthogonal. The coexistence of two modes was observed in the experiment. The first mode suppression in the low-u_0 low-h region may be attributed to a nonlinear effect; however, further discussion is beyond the scope of the present study. Aside from this discrepancy, the analytical result agrees fairly well with the experimental result, particularly in the first mode of Case A. Qualitative agreement is good even in the worst case; for example, the upper and lower u_0 limits of the region exist, and the lower limit decreases in Case D.

However, the calculated oscillating region is narrower than the experimental region in Cases C and D and in higher modes. Although the supplied energy is positive in the calculated boundary, the sloshing can grow only in the narrower region in the experiment due to the energy dissipation. Taking the dissipation into account, the calculated lower u_0 limit should be much lower. The discrepancy is attributed primarily to underestimation of the phase lag due to a simplification in the model. A marked discrepancy is present over the entire boundary in Cases C and D and in higher modes, in which the assumption of a small jet diameter compared to the sloshing wavelength is not valid. The attenuation of pressure imbalance by wave propagation cannot be neglected when the jet diameter is not sufficiently small compared to the sloshing wavelength.

Although we simplified the phenomenon drastically in the analysis by replacing the velocity distribution of the jet with a jet of uniform profile, the analytical result agrees fairly well with the experimental result, indicating the validity of the model shown in Figure 12.

4.4. Comparison to Oscillations in the Rectangular Tank

The round jet does not partition the cylindrical tank into two sectors. Sloshing motion is only slightly impeded by the jet; therefore, the frequency is governed by sloshing motion. However, the energy supply mechanism is basically the same as that of jet-flutter, which is quite different from that of self-induced sloshing in the rectangular tank. The feedback model in Figure 12 is basically identical to that developed to explain jet-flutter. Thus, this phenomenon is thought to be the same as jet-flutter from the viewpoint of the energy supply mechanism.

5. CONCLUSION

Self-induced sloshing was observed in a cylindrical tank having an upward round jet on the axis. Characteristics of the sloshing are as follows: (a) the sloshing mode always has one diametric node; (b) the sloshing appears when the inlet velocity exceeds a certain value, which depends on the inlet-surface distance; (c) a lower mode appears with increasing inlet-surface distance and jet velocity; (d) a surface swell is formed at the jet impingement point when sloshing occurs.

The energy supply mechanism for sloshing is considered to have the following characteristics: (i) a lateral pressure difference deflects the jet, resulting in the displacement of the surface impingement point; (ii) transformation of the jet-induced swell cannot follow the lateral movement of the jet instantaneously; (iii) the imbalance causes a lateral pressure difference: a low pressure at the front and a high pressure at the rear; (iv) when the pressure difference supplies energy to the sloshing, the sloshing grows.

The pressure-difference jet–deflection relationship, the phase relation between the swell motion and the pressure difference, and the oscillating region were calculated based on the above model. The results agree with the experimental findings, which supports the validity of the model.

References

Abramovich, G. N. 1963 *The Theory of Turbulent Jets*, p. 75. Cambridge, MA: MIT Press.

Abramson, H. N., Chu, W. H. & Kana, D. D. 1966 Some studies of nonlinear lateral sloshing in rigid containers. *Journal of Applied Mechanics* **33,** 777–784.

Blake, W. K. 1986 *Mechanics of Flow-Induced Sound and Vibration*, Vol. I, p. 130. Orlando, FL: Academic Press.

Fukaya, M., Madarame, H. & Okamoto, K. 1996 Growth mechanism of self-induced sloshing caused by vertical plane jet. *Proceedings ASME–JSME 4th International Conference on Nuclear Engineering* (eds A. S. Rao, R. B. Duffey & D. Elias), New Orleans, LA, Vol. 1, pp. 781–787.

Houard, S., Daviaud, F. & Bergé, P. 1996 Phase-locking modes in a bidimensional network of coupled water jets. *Physica D* **99,** 318–338.

Lamb, H. 1932 *Hydrodynamics*, 6th edition, 358. Cambridge: Cambridge University Press.

Madarame, H. & Iida, M. 1998 Mechanism of jet-flutter: self-induced oscillation of an upward plane jet impinging on a free surface. *JSME International Journal, Series* B **41,** 610–617.

Madarame, H., Okamoto, K. & Iida, M. 1995 Self-induced sloshing caused by an upward round jet impinging on the free surface. In *Fluid-Sloshing and Fluid-Structure Interaction* (ed. D. C. Ma), PVP Vol. 314, pp. 27–33. New York: ASME.

NYBORG, W. L. 1954 Self-maintained oscillations of the jet in a jet-edge system. I. *Journal of the Acoustical Society of America* **26,** 174–182.

OKAMOTO, K. & MADARAME, H. 1998 Fluid dynamics of a free surface in liquid metal fast breeder reactors. *Progress in Nuclear Energy* **32,** 195–207.

APPENDIX A: NOMENCLATURE

A	representative surface amplitude
c	protruded length of inlet into tank
D	inner diameter of inner cylinder
d	inner diameter of inlet pipe
f	frequency
g	gravitational acceleration
H	water depth
h	distance from inlet to free surface, $H - c$
p	pressure
q	amount of imbalance generated
R	inner radius of inner cylinder
U	representative x-direction velocity component of jet
u_0	jet inlet velocity
u_h	jet velocity at surface position
u_m	velocity at jet axis
V	representative y-direction velocity component of jet
εA	amplitude of jet displacement at surface position
ζ	vertical motion of sloshing surface
η	lateral displacement of jet
η_h	lateral displacement of jet at surface position
ρ	water density
σ	assumed radius of jet at surface position
φ_1	phase lag of η_h behind acceleration oscillation
φ_2	phase lag of q behind η_h
ω	angular frequency